Biochimica et Biophysica Acta 1847 (2015) 558–564

Contents lists available at ScienceDirect

Biochimica et Biophysica Acta

journal homepage: www.elsevier.com/locate/bbabio

Directly probing redox-linked quinones in photosystem II membrane fragments via UV resonance Raman scattering

Jun Chen [a,b,*], Mingdong Yao [a], Cynthia V. Pagba [c], Yang Zheng [a], Liping Fei [a], Zhaochi Feng [b], Bridgette A. Barry [c]

[a] Dalian National Laboratory for Clean Energy, Dalian Institute of Chemical Physics, Chinese Academy of Sciences, Dalian 116023, China
[b] State Key Laboratory of Catalysis, Dalian Institute of Chemical Physics, Chinese Academy of Sciences, Dalian 116023, China
[c] School of Chemistry and Biochemistry and the Petit Institute for Bioengineering and Bioscience, Georgia Institute of Technology, Atlanta, GA 30332, United States

ARTICLE INFO

Article history:
Received 9 December 2014
Received in revised form 19 February 2015
Accepted 10 March 2015
Available online 17 March 2015

Keywords:
Carbonyl bond
Photosynthesis
Proton transfer
Electron transfer
Lipid membrane
Protein dynamics

ABSTRACT

In photosynthesis, photosystem II (PSII) harvests sunlight with bound pigments to oxidize water and reduce quinone to quinol, which serves as electron and proton mediators for solar-to-chemical energy conversion. At least two types of quinone cofactors in PSII are redox-linked: Q_A, and Q_B. Here, we for the first time apply 257-nm ultraviolet resonance Raman (UVRR) spectroscopy to acquire the molecular vibrations of plastoquinone (PQ) in PSII membranes. Owing to the resonance enhancement effect, the vibrational signal of PQ in PSII membranes is prominent. A strong band at 1661 cm^{-1} is assigned to ring C═C/C═O symmetric stretch mode (ν8a mode) of PQ, and a weak band at 469 cm^{-1} to ring stretch mode. By using a pump-probe difference UVRR method and a sample jet technique, the signals of Q_A and Q_B can be distinguished. A frequency difference of 1.4 cm^{-1} in ν8a vibrational mode between Q_A and Q_B is observed, corresponding to ~86 mV redox potential difference imposed by their protein environment. In addition, there are other PQs in the PSII membranes. A negligible anharmonicity effect on their combination band at 2130 cm^{-1} suggests that the 'other PQs' are situated in a hydrophobic environment. The detection of the 'other PQs' might be consistent with the view that another functional PQ cofactor (not Q_A or Q_B) exists in PSII. This UVRR approach will be useful to the study of quinone molecules in photosynthesis or other biological systems.

1. Introduction

Quinones play vital roles in biological energy transduction [1]. As an example, plastoquinones (PQs) serve as the terminal electron and proton mediators in photosystem II (PSII) [2–4], which is found in cyanobacteria, plants, and algae. PSII harvests sunlight with bound pigments, including chlorophyll (Chl) to drive a series of electron transfer reactions.

On the stromal side of PSII membrane, the electron transfer cofactor Q_A (a PQ) is reduced to Q_A^- in 400 ps by the primary electron acceptor $Pheo^-$ [5], and then Q_A^- reduces the neighboring Q_B (another PQ) in 200–400 μs [6]. Although Q_A and Q_B are chemically identical as PQ, their physiological redox processes are different. Q_A is only one-electron reduced, whereas Q_B accepts two electrons and two protons converting to plastoquinol PQH_2, which is then released from PSII [2,4].

As revealed by the X-ray crystallographic structure of cyanobacterial PSII (Fig. 1a) [7], cofactors Q_A and Q_B are situated symmetrically to the non-heme iron which binds with a bicarbonate and four histidine residues. The π-planes of their quinonoid rings are parallel with C═O pointing toward each other. The theoretical calculations based on the detailed crystalline structure suggest that the carbonyl groups of Q_B play important roles in proton coupled electron transfer [8]. Subtle structural changes imposed by the protein environment are not distinguishable from current X-ray crystallographic data.

To obtain more information about the structure and function of quinones, Raman spectroscopy is an incisive technique for studying aqueous biological samples giving fingerprint information on the chemical bond vibrations of target molecules [9,10]. Previous Raman investigations of benzoquinone (BQ), BQ anion radicals, and benzoquinols have shown that the C–O associated vibrations of these three species are distinguishable [11–13]. For example, reduction of BQ to BQ^- causes the ν8a mode (C═C/C═O stretch) shift from 1668 cm^{-1} to 1619 cm^{-1} [13]. Excitation at the wavelength of 441.6, 363.8, 351.1 or 325 nm, taking advantage of the large shifts in UV–visible absorption bands observed with reduction of quinones, shows clear resonance Raman

Abbreviations: UVRR, ultraviolet resonance Raman; PSII, photosystem II; SDS-PAGE, sodium dodecyl sulfate polyacrylamide gel electrophoresis; Tris–HCl, 2-amino-2-(hydroxymethyl)-1,3-propanediol hydrochloride; EDTA, tetrasodium ethylenediaminetetraacetic acid; MES, 2-(N-morpholino) ethanesulfonic acid; DCMU, 3-(3,4-dichlorophenyl)-1,1-dimethylurea; PQ, plastoquinone; decyl-PQ, decyl-plastoquinone; OTG, n-octyl-β-D-thioglucoside; LHC, light harvesting complex; FTIR, Fourier transform infrared spectroscopy; HPLC, high-performance liquid chromatography

* Corresponding author at: Dalian National Laboratory for Clean Energy, Dalian Institute of Chemical Physics, Chinese Academy of Sciences, Dalian 116023, China.
E-mail address: junchen@dicp.ac.cn (J. Chen).

http://dx.doi.org/10.1016/j.bbabio.2015.03.002
0005-2728/

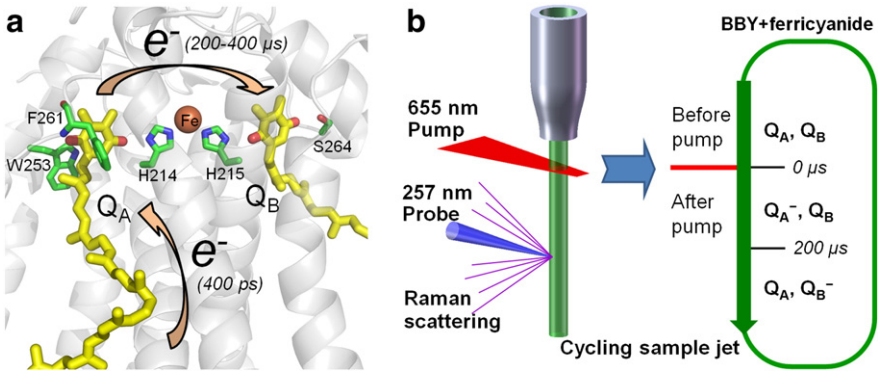

Fig. 1. (a) The local environment of the cofactors Q_A and Q_B in cyanobacterial PSII (PDB ID: 3ARC, reference [7]). The time constants for electron transfer to Q_A, and from Q_A to Q_B, are indicated. (b) Schematic of the pump-probe approach for UVRR measurements of PSII samples. The liquid sample was forced through a nozzle, forming a jet. The continuous-wave laser with 655 nm wavelength was focused as a line cutting the sample jet to pump the light-driven physiological processes in PSII samples. The Raman scattering excited with a 257 nm continuous-wave laser was exploited to probe the molecular vibrations of the samples. On the right side, the states of Q_A and Q_B cofactors before and after pump are indicated.

signals of the reduced BQ species (BQ^-, BQH^- and BQ^{2-}) [12]. In contrast, excitation at a shorter wavelength of 245 nm gives the greatly responsive resonance Raman signal of BQ [11]. These data were obtained on model compounds in aqueous solution or organic solvents. Importantly, previous researches on model quinone derivatives with vibrational spectroscopy reveal that the carbonyl vibration of quinone is related to the induction effect and the redox potential [13–15].

Excitation with proper UV light enhances Raman scattering from aromatic molecules, and shifts the Raman signal to UV region therefore avoiding most fluorescence interference especially from pigment molecules in protein complex, such as PSII [16] and PSI [17]. Similarly, PQ possesses a strongest UV absorption band at around 255 nm [18,19], whereas, reduction of PQ shifts its maximum absorption to longer wavelengths as 288, 320, 412 and 436 nm [18–21]. To obtain more information concerning the chemical bonds of the redox-linked quinone cofactors of PSII, we exploited 257-nm ultraviolet resonance Raman (UVRR) spectroscopy with a sample jet technique to characterize the PSII enzyme (Fig. 1b), because 257-nm excitation is expected to resonantly enhance the spectral contribution of PQ. However, the signals of reduced PQ species (e.g., PQ^- and PQH_2) are not expected to be resonantly enhanced because their electronic transition absorption bands are far away from the Raman excitation wavelength of 257 nm [18–21].

2. Materials and methods

2.1. PSII samples

The PSII membranes (referred to as BBY) were isolated from fresh spinach leaves as described previously [22,23]. Their final Chl concentrations were in the range 2.2–2.7 mg Chl mL^{-1}, and oxygen evolution rates were over 800 μmol O_2 (mg Chl)$^{-1}$ h^{-1} [24]. The Mn-depleted PSII membranes (denote as Mn-depleted BBY), in which the manganese oxide cluster was removed as well as extrinsic PsbO, PsbP and PsbQ subunits, were prepared by incubation of BBY in an equal volume of a buffer containing 1.6 M Tris–HCl (pH 8.0) and 4 mM EDTA in light [25]. Their final Chl concentrations were ~2.0 mg Chl mL^{-1}. The PSII core complexes, in which LHCII, CP26, CP29 and part of PsbP and PsbQ subunits were removed, were obtained by the treatment of BBY with detergent OTG [26]. Their final Chl concentrations were ~0.26 mg Chl mL^{-1} and oxygen evolution rates were ~1360 μmol O_2 (mg Chl)$^{-1}$ h^{-1}. All these samples were individually suspended in an SMN buffer (400 mM sucrose, 50 mM MES-NaOH, 15 mM NaCl, pH 6.0), and were frozen at −70 °C until use. The polypeptide compositions of these PSII samples were confirmed by SDS-PAGE [27].

2.2. UV–visible spectra

To record the absorption bands corresponding to the electronic transitions of PSII complexes, UV–visible spectroscopy (spectrometer: Cary 50, Varian, USA) has been exploited. The PSII samples were diluted in the SMN buffer, and this buffer was the reference solution. The parameter settings were: scan speed, 120 nm min^{-1}; sampling interval, 1.0 nm; and averaging time, 0.5 s. These parameter settings were also applied to the measurement of decyl-plastoquinone (decyl-PQ) which was dissolved in ethanol.

2.3. UVRR setup

UV resonance Raman measurements were performed by using a home-built instrument. The continuous-wave laser line of 257 nm wavelength (LEXEL 95, Cambridge, USA) was selected as Raman excitation source. In a backscattering collection mode, the laser beam was defocused on the sample with a UV objective (OFR division of Thorlabs Inc., USA), and Raman scattering from the sample was collected by the same objective and passed through edge filters (Semrock, USA) that block Rayleigh scattering. The Raman signal was further focused into a monochromator with 500 mm focal length (SR-500, Andor Technology, UK), thus was dispersed onto a UV-enhanced CCD detector (Newton 940-BU2, Andor Technology, UK). In order to capture high signal-to-noise spectra, the UV objective with a numerical aperture of 0.32 and an 8.5 mm working distance was adopted for high signal collection efficiency and for sufficient space in holding the sample jet; a 3600 groove mm^{-1} ruled grating which blazed at 240 nm was used for the dispersion of Raman signal; the wavelength responses of all mirrors and lens are specific for UV light of ~250 nm. Prior to the UVRR measurements, the spectral linearity was calibrated with the spectral lines of a mercury lamp, and the accuracy was calibrated with the UV Raman signal of a diamond. The spectral parameters were determined to be as follows: spectral resolution, 3.5 cm^{-1}; data interval, 1.1 cm^{-1}; and spectral cut-off frequency, <300 cm^{-1}. The frequency reproducibility for measurements was better than 0.1 cm^{-1}, which can be indicated by successive measurements of cyclohexane (see Fig. S1). This good reproducibility was also confirmed with the difference spectrum of successive measurements of PSII samples (see Fig. S2).

2.4. UVRR measurements

UVRR measurements were conducted at room temperature. Samples were recirculated in a flow cell with a nozzle, forming a liquid

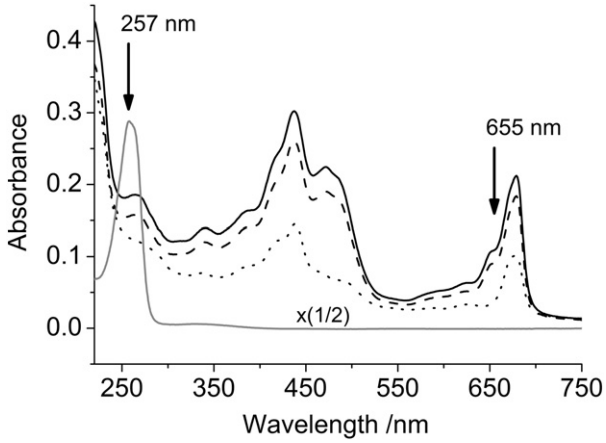

Fig. 2. UV–visible absorption spectra of (solid black line) BBY, (dash line) Mn-depleted BBY, and (dot line) PSII core complex, with chlorophyll concentrations of 2.4, 1.9 and 0.63 μg Chl mL^{-1}, respectively. For comparison, UV–visible absorption spectrum of (solid gray line) 100 μM decyl-PQ is provided, and its absorbance is divided by 2 for presentation purpose. The arrows mark the wavelengths of the Raman excitation source (257 nm) and the pump source (655 nm).

jet with an ~4.1 m s^{-1} flow rate passing through the UV probe spot [16,17]. It took 13 s $cycle^{-1}$ for 1.0 mL of sample. The power of the UV probe was around 360 μW, and the exposure time was 20 min for each spectrum except that specifically mentioned. After UVRR measurements, the BBY samples retained oxygen evolution rates of >800 μmol O_2 $(mg\ Chl)^{-1}$ h^{-1}. For the pump-probe measurements (see Fig. 1b), a pump beam with 655 nm wavelength was used to trigger the light-driven physiological processes in PSII samples. This pump beam of 30 mW was focused as a line cutting the sample jet with a specific distance relative to the UV probe spot. The transit time between the red pump and the UV probe was estimated to be 240 μs per 1.0 mm distance. To achieve the difference spectra, samples were measured at first by using 257-nm Raman probe only, and then were measured by using 655-nm pump and 257-nm Raman probe. Each measurement took 20 min except that specifically mentioned. The Raman signal of water was used as an internal standard for obtaining all difference spectra in this work. Note that no specific chemical was added as an internal standard during the Raman measurements.

3. Results

3.1. 257-nm resonance Raman spectra of PSII samples

In accordance with the UV absorption features (see Fig. 2) of BBY, the 257-nm excitation resonantly enhances Raman signals of some types of molecules in BBY, exhibiting rich vibrational bands in the region <1700 cm^{-1} (see Fig. 3). To achieve the assignments of these vibrational bands, 20 types of amino acids have been investigated, only tryptophan is significantly enhanced by 257-nm excitation as shown in Fig. 3. Based on the spectral features of tryptophan, some (marked with solid circle in Fig. 3a) of those vibrational bands of BBY are therefore attributed to Trp residues, and their normal mode assignments are listed in Table S1.

Two other PSII samples were also measured: one is Mn-depleted BBY in which the Mn_4CaO_5 cluster was removed as well as extrinsic PsbO, PsbP and PsbQ subunits, and the other is PSII core complex in which the outer subunits including LHCII, CP26 and CP29, and part of PsbP and PsbQ subunits were removed. The Chl concentrations of these measured samples are 2.2–2.7, 2.0 and 0.26 mg Chl mL^{-1} for BBY, Mn-depleted BBY and PSII core complex, respectively. According to 274 Chls per PSII reaction center for BBY [20] and 35 Chls per cyanobacteria PSII core complex [7], these measured PSII samples in Fig. 3 have a close concentration of reaction center. Compared to BBY, the spectrum (Fig. 3b) of Mn-depleted BBY exhibits similar bands and a similar shape. However for the PSII core complex, the Trp bands become more prominent; the relative intensity of other bands to the Trp bands decreases significantly, except for the band at 1661 cm^{-1} (see Fig. 3c). This comparison indicates that the molecule responsible for the 1661 cm^{-1} band must be a common component of these three PSII samples.

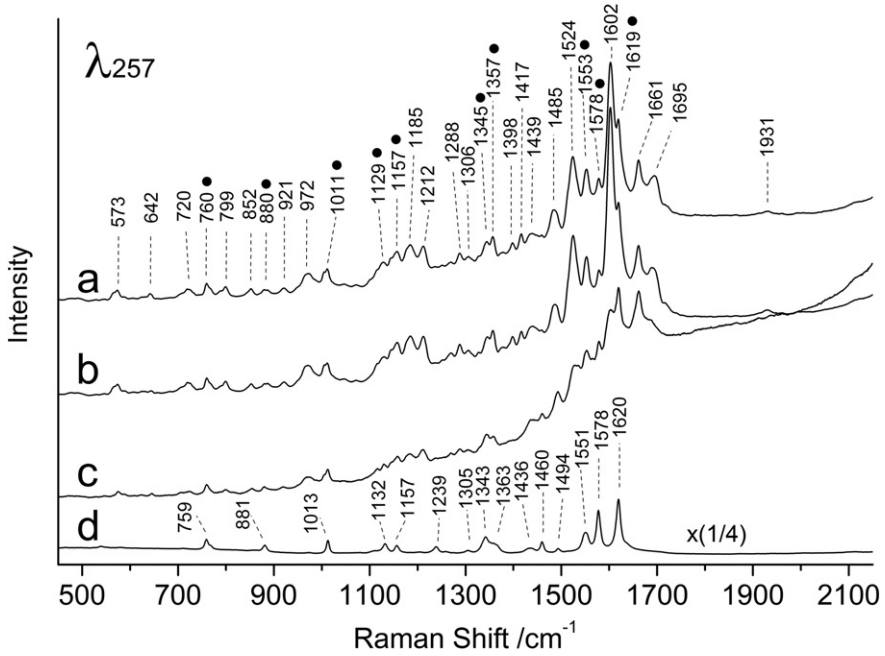

Fig. 3. UVRR spectra of (a) BBY, (b) Mn-depleted BBY, and (c) PSII core complex, excited with a 257 nm probe beam. No exogenous electron acceptor was added to these PSII samples. The spectra (a), (b) and (c) are the average of 10, 10, and 3 data sets, respectively. The Chl concentrations of BBY are 2.2–2.7 mg Chl mL^{-1}; Mn-depleted BBY, 2.0 mg Chl mL^{-1}; PSII core complex, 0.26 mg Chl mL^{-1}. For comparison, (d) UVRR spectrum (with exposure time of 10 min) of 2.0 mM tryptophan dissolved in a 5 mM MES-NaOH buffer (pH 6.0) is provided, and its spectral intensity is divided by 4. For clarity, these spectra are offset along the *y* axis.

3.2. Pump-probe UVRR measurements of PSII samples with no exogenous electron acceptor

Further, a pump-probe approach (see Fig. 1b) was conducted to characterize intensity changes and frequency shifts in the signal caused by charge separation changes in PSII. The illumination of a 655-nm laser was adopted as the pump to initialize charge separation before the flowing sample passed through the Raman probe. In comparison with the probe-only spectrum (Fig. 4a), we can see an obvious intensity drop in the 1661 cm^{-1} band, in the pump-plus-probe spectrum (Fig. 4b) when the BBY sample without added any exogenous electron acceptors. The difference spectrum (Fig. 4c) clearly presents a sharp strong band at 1661 cm^{-1} and several weak bands at 469, 1600, and 2130 cm^{-1}. This result indicates that the 1661 cm^{-1} band is likely attributable to a PSII cofactor.

Among the cofactors of PSII, the Raman scattering of PQs is expected to be resonantly enhanced at 257-nm excitation, on the basis of their UV absorption features [18,19]. To distinguish the spectral contribution from PQs, a PQ derivative, decyl-PQ, was characterized for comparison since decyl-PQ has similar spectral features as PQ [21]. As shown in Fig. 2, decyl-PQ possesses a prominent absorption band at around 257 nm. In accordance with its UV absorption features, decyl-PQ presents a remarkable resonance Raman effect at 257-nm excitation, showing a very strong band at 1663 cm^{-1} and two weak bands at 469 and 2127 cm^{-1} (see Fig. 4d). These Raman spectral features are similar to those of the pump-probe difference spectrum (Fig. 4c) of BBY. Therefore, this comparison demonstrates that the vibrational bands at 469, 1661 and 2130 cm^{-1} (in Fig. 4c) are attributable to PQs in PSII membranes.

The presence of the PQ signal in the pump-probe difference spectrum of BBY suggests that the PQs are reduced after the red light illumination, because some their reduced forms PQ^{-} and PQH_2 absorb maximally at 320 nm and 288 nm, respectively [18,19], and are not expected to be detectable with 257-nm Raman excitation without resonance effect. Pump-probe measurements were also performed on the PSII core complex. Similarly, the PQ signal is dominated in the pump-probe difference spectrum of the PSII core complex (data not shown).

3.3. Time-resolved pump-probe UVRR measurements of BBY with added ferricyanide

As shown in Fig. 1b, to distinguish the Q_A and Q_B signals, different delay times between the pump and probe were used for the difference UVRR measurements of BBY, on the basis of the redox kinetic analysis: Q_A reduction to Q_A^- occurs in hundreds of picoseconds [5,28], Q_A^- then reduces Q_B in 200–400 μs [6]. In addition, an exogenous electron acceptor, potassium ferricyanide, was added to the BBY sample for converting the reduced PQ species back to the neutral form. Note that the sample was circulating through the pump and probe laser beams during the measurements.

When the sample is illuminated with the pump beam at ~200 μs prior to the Raman probe, the difference spectrum (Fig. 5a) shows positive bands at 1520, 1600 and 1659 cm^{-1}, and negative bands at 2052 and 2088 cm^{-1}. When the pump beam is placed at ~900 μs before the probe beam, the difference spectrum (Fig. 5b) exhibits similar bands as those in Fig. 5a. When the sample is illuminated with the pump beam at ~700 μs after the Raman probe, the difference spectrum (Fig. 5c) shows the positive 1520 and 1600 cm^{-1} bands, and the negative 2052 and 2088 cm^{-1} bands, however, the 1659 cm^{-1} band is negligible. A control difference spectrum (Fig. 5d) is also generated by subtraction of one-half of a probe-only data set from the other half of that same set. The presence of only noise baseline in Fig. 5d demonstrates that there is no significant actinic effect from the Raman probe. Comparison of these pump-probe difference spectra (Fig. 5a, b

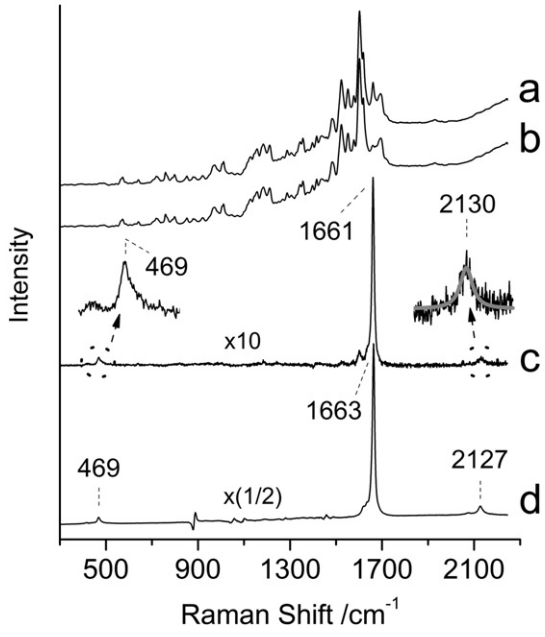

Fig. 4. Pump-probe UVRR measurements of BBY without added any exogenous electron acceptors. (a) Probe-only spectrum (Raman probe, 257 nm). (b) Pump-plus-probe spectrum (pump, 655 nm; Raman probe, 257 nm). The pump beam was placed at ~200 μs prior to the probe beam. The spectra (a) and (b) are each the average of 10 data sets. The Chl concentrations of BBY are 2.2–2.7 mg Chl mL^{-1}. (c) Difference spectrum obtained by subtracting spectrum (b) from (a). For the subtraction, the Raman signal of water was used as an internal standard. Insets zoom in spectrum (c) in two different frequency regions and its Lorentzian fitting (gray line) at around 2130 cm^{-1}. For comparison, UVRR spectrum (d) (with exposure time of 10 min) of 500 μM decyl-PQ dissolved in ethanol is provided with the subtraction of the ethanol signal. For presentation purpose, the intensity of spectrum (c) is multiplied by 10, and that of spectrum (d) is divided by 2.

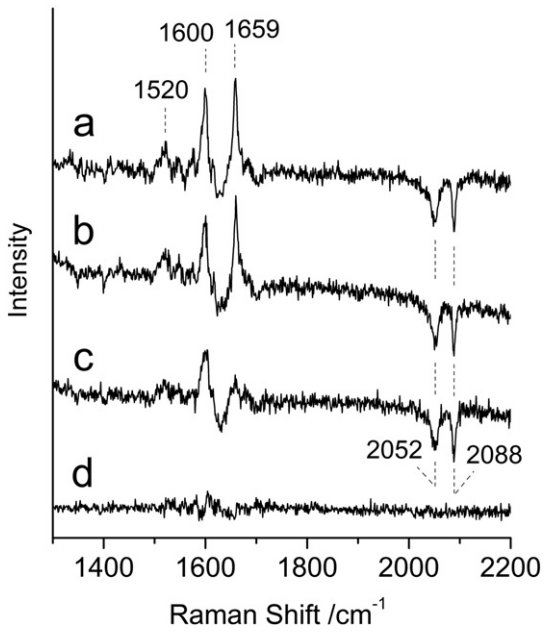

Fig. 5. Delay time dependent UVRR difference spectra of BBY with added the exogenous electron acceptor, potassium ferricyanide (3 mM). The difference spectra were obtained by subtracting the pump-plus-probe spectrum (pump, 655 nm; Raman probe, 257 nm) from the probe-only spectrum (Raman probe, 257 nm). In spectrum (a), (b) and (c) measurements, the pump beam was placed at ~200 μs and ~900 μs prior to the probe beam, and ~700 μs after the probe beam, respectively. (d) A control difference spectrum which is generated by subtraction of the last 10 min from the first 10 min of probe-only data collection on the same sample. For all the subtractions, the Raman signal of water was used as an internal standard, and the original probe-only spectra were normalized in intensity. All the spectra are the average of 12 data sets. The Chl concentrations of BBY are 2.2–2.7 mg Chl mL^{-1}.

and c) with Fig. 5d indicates that those detected bands result from pump light-driven processes.

The assignments of the 1520 and 1600 cm^{-1} bands are unknown. The two negative bands at 2052 and 2088 cm^{-1} are attributed to the generated ferrocyanide as demonstrated by its UVRR spectrum (Fig. S3). The formation of ferrocyanide indicates that the present ferricyanide accepts electron from the reduced PQ species at the end of the light-driven electron transfer chain. According to the results from pump-probe UVRR measurements of BBY without added ferricyanide (see Fig. 4), the positive ~1659 cm^{-1} band in Fig. 5 can be assigned to PQ signal. In addition, the absence of the PQ band in Fig. 5c is in agreement with the conversion of the reduced PQ species back to the neutral forms for the sample with added ferricyanide after one cycle flowing time (13 s) in the dark.

Fig. 6 shows the expanded spectra of Fig. 5a and b in the PQ band and ferrocyanide band regions. We can see that there is a frequency shift for the PQ band while the ferrocyanide band locates at exactly the same frequency. The accurate positions of the PQ bands are at 1658.7 and 1660.1 cm^{-1} for the pump-probe difference spectra with delay times of ~200 and ~900 μs, respectively. In addition, the PQ band on the pump-probe difference spectrum of BBY with no ferricyanide locates at 1661.2 cm^{-1} (blue line in Fig. 6). The band positions are determined by Lorentzian fitting. Note that the spectral reproducibility is better than 0.1 cm^{-1} during the measurements (see Fig. S1). This good reproducibility can be also demonstrated from the flat difference spectra of successive measurements of PSII samples (see Figs. S2 and 5d). Such small frequency change could be distinguished since bands cover much wide frequency ranges (tens of wavenumbers), although the spectral resolution is 3.5 cm^{-1} and data interval is 1.1 cm^{-1}.

As well known, the primary charge separation in PSII is extremely fast, the electron transfer to Q_A forming Q_A^- occurs in hundreds of picoseconds after light collection [5,28]. By measuring the Chl fluorescence yield transients, it is found that time constant is 200–400 μs for electron transfer from Q_A^- to Q_B forming Q_A and Q_B^-, and 600–800 μs for electron transfer from Q_A^- to Q_B^- [5,6]. According to this kinetic analysis, the band at 1658.7 cm^{-1} which is detected with time delay of ~200 μs (see Fig. 5a and black line in Fig. 6) should be mainly attributed to Q_A, the band at 1660.1 cm^{-1} which is detected with time delay of ~900 μs (see Fig. 5b and orange line in Fig. 6) is attributed to Q_B. Likewise, the band at 1661.2 cm^{-1} (see Fig. 4c and blue line in Fig. 6) is mainly attributed to the 'other PQs' because PQs act as the terminal electron acceptor in the absence of the exogenous ferricyanide, and this band is much stronger than the Q_A band or the Q_B band.

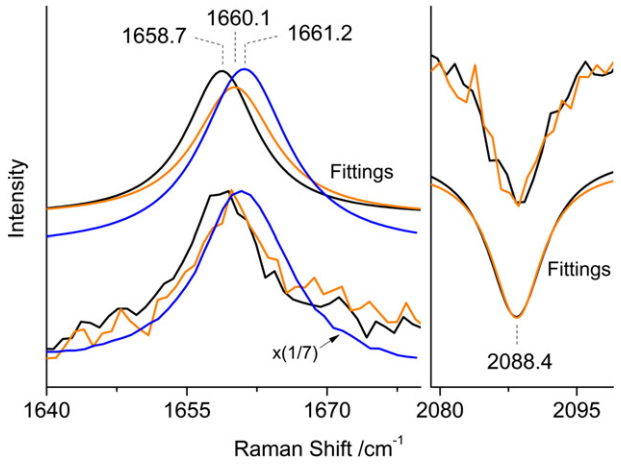

Fig. 6. Expanded view of (black line) Fig. 5a and (orange line) Fig. 5b and their Lorentzian fittings in two frequency regions. For comparison, (blue line) the pump-probe difference spectrum of BBY without added any exogenous electron acceptors is reproduced from Fig. 4c, and its intensity is divided by 7 for presentation purpose. All their original probe-only spectra were normalized in intensity for achieving difference spectra. For clarity, the fitting spectra are offset along the *y* axis.

3.4. Pump-probe UVRR measurements of BBY with added DCMU

On the other hand, a control PSII sample was also investigated with the addition of inhibitor DCMU, where the presence of DCMU can block the electron transfer from Q_A to Q_B and upshifts the redox potential of Q_A by 52 mV [29,30]. With the pump beam at ~200 μs prior to the Raman probe, the difference Raman spectrum (Fig. 7) of this control sample shows a band at 1659.9 cm^{-1}. This band must be attributed to Q_A in that situation, because the reduction of Q_B is terminated in the presence of DCMU.

3.5. Reduction of decyl-PQ in BBY measured by Pump-probe UVRR

An experiment has also been carried out to analogize the reduction of PQs in the BBY. After the pump-probe measurements of BBY without added ferricyanide, 30 μM decyl-PQ was added to the sample solution, and then the pump-probe measurements were performed again. In this experiment, it is assumed that decyl-PQ is a facile electron acceptor and will substitute for PQ. Shown in Fig. 8, the UVRR spectra were achieved to monitor the quinone band (at around 1661 cm^{-1}) change during these treatments. Similar to the PQs (see Fig. 8a and b), most of decyl-PQs (see Fig. 8c and d) can be reduced under red light illumination on the BBY solution. Both pump-probe difference spectra (Fig. 8e and f) show similar spectral features each other. This comparison demonstrates that there are some 'other PQs' within the PSII membranes and they are also contributed to the 1661 cm^{-1} band of the probe-only UVRR spectrum of BBY (Figs. 4a and 8a). Since Q_A, Q_B and the 'other PQs' are chemically identical and behave with similar Raman spectra, their Raman cross-section should be approximately equal.

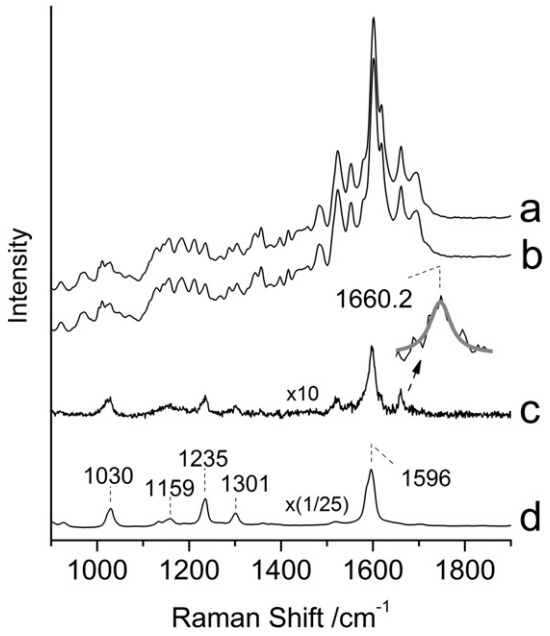

Fig. 7. Pump-probe UVRR measurements of BBY with added inhibitor DCMU (100 μM). (a) Probe-only spectrum (Raman probe, 257 nm). (b) Pump-plus-probe spectrum (pump, 655 nm; Raman probe, 257 nm). The pump beam was placed at ~200 μs prior to the probe beam. The spectra (a) and (b) are each the average of 12 data sets. (c) Difference spectrum obtained by subtracting spectrum (b) from (a). Inset zooms in spectrum (c) and its Lorentzian fitting (gray line) at around 1660 cm^{-1}. The Chl concentrations of BBY are 2.2–2.7 mg Chl mL^{-1}. For comparison, (d) UVRR spectrum (with exposure time of 10 min) of 500 μM DCMU dissolved in methanol is provided with the subtraction of the methanol signal. For presentation purpose, the intensity of spectrum (c) is multiplied by 10, and spectrum (d) divided by 25.

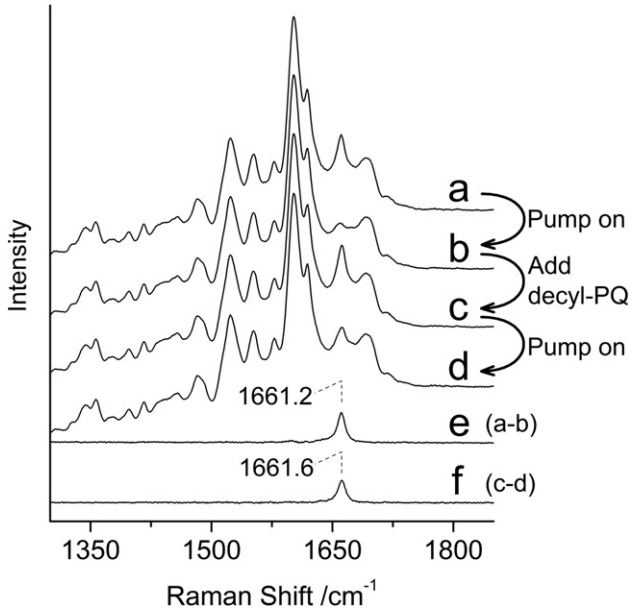

Fig. 8. Monitoring the reduction of quinones in BBY by UVRR spectroscopy. (a) Probe-only measurement of BBY (1.4 mg Chl mL^{-1}) without added any exogenous electron acceptors. (b) Successive pump-plus-probe measurement (pump, 655 nm; Raman probe, 257 nm) after (a). (c) Successive probe-only measurement of the sample with added 30 μM decyl-PQ. (d) Successive pump-plus-probe measurement after (c). (e) Difference spectrum obtained by subtracting spectrum (b) from (a). (f) Difference spectrum obtained by subtracting spectrum (d) from (c). The pump beam was placed at ~200 μs prior to the probe beam. The exposure time of each measurement is 10 min. All these spectra are the average of 5 independent data sets.

However, without 257-nm Raman spectrum of purified PQ with a certain concentration, it is difficult to determine each contribution from Q_A, Q_B or the 'other PQs' in the probe-only UVRR spectrum of BBY.

3.6. Theoretical calculations of PQ vibrations

By using 257-nm UVRR spectroscopy, we can probe the PQ cofactors in plant PSII membranes. To identify the specific chemical bond contributions of these PQ vibrational bands, a calculation by B3LYP density functional method with a 6-311++G(d,p) basis set was performed on a model quinone molecule, 2,3-dimethyl-5-propenyl-1,4-benzoquinone (see Fig. S4), which has the isoprenyl chain replaced by a propenyl group. The quantum chemistry program *Gaussian 03* was used for this calculation [31]. According to the calculated vibrational modes and their frequencies and Raman activities (Table S2) of this model quinone, for PQ, the 1661 cm^{-1} band is assigned to ring C═C/C═O symmetric stretch mode (ν8a mode), the 469 cm^{-1} band to ring stretch mode, and the 2130 cm^{-1} band to the combination mode of these two modes at 1661 and 469 cm^{-1}.

4. Discussion

The C═O bonds directly take part in the reduction of Q_A to Q_A^- and the reduction of Q_B finally to PQH_2. Indicated from Fig. 6, there is a frequency difference, 1.4 cm^{-1}, in ν8a mode between Q_A and Q_B, and 1.1 cm^{-1} between Q_B and the 'other PQs'. Researches on model quinone derivatives have revealed that the C═O vibrational frequency of quinone is related to the reduction potential due to induction effect [14,15]. By investigating solvent effect of 1,4-benzoquinone, Zhao and Kitagawa presented the cyclic voltammogram and Raman data, indicating a relationship of 62 ± 15 mV per wavenumber (cm^{-1}) between the reduction potential of 1,4-benzoquinone and its vibrational ν8a mode (see Fig. S5) [13]. According to this relationship, 1.4 cm^{-1} difference in ν8a mode between Q_A and Q_B suggests that the specific induction from protein environment imposes an alteration of ~86 mV in the redox capability between Q_A and Q_B. This redox potential difference (~86 mV) deduced by our UVRR investigation is consistent with that (around 80 mV) based on the equilibrium constant analysis between Q_A and Q_B from thermoluminescence studies [32–34]. Likewise, the addition of DCMU giving rise to a red shift (~1.2 cm^{-1}) in ν8a mode of Q_A indicates an upshift of the redox potential of Q_A. This result is also in agreement with the measurements by a thermoluminescence approach [29,30].

Based on the crystal structure of cyanobacterial PSII [7] as shown in Fig. 1a, the carbonyl oxygens of Q_A are each H-bonded to the N_δ-atom of His214 and to the amide group of Phe261, and the quinonoid ring of Q_A is close to a π-stack situation with Trp253; the carbonyl oxygens of Q_B are also H-bonded, one to His215 and the other to Ser264. This structural pattern for Q_A and Q_B suggests that these H bonds are likely the major factors influencing the redox potential alteration of Q_A and/or Q_B. As detected only one C═C/C═O stretch band for Q_A and Q_B (see Fig. 5) like free PQ, this implies that the interaction between the protein microenvironment and both C═O groups of Q_A and/or Q_B is weak for plant PSII. In contrast, for bacteria *Rhodobacter sphaeroides* R26 reaction center, a drastic frequency downshift of the 4-C═O vibration of a ubiquinone-10 at Q_A site as compared with the 1-C═O vibration is detected [35], indicating a strong interaction between the protein microenvironment and the 4-C═O group of Q_A rather than the 1-C═O group for *Rhodobacter sphaeroides* reaction center.

For the 'other PQs' detected by pump-probe difference measurements (Fig. 4c) of BBY samples without added ferricyanide, the frequency of the combination band at 2130 cm^{-1} is approximately equal to the frequency sum of the two fundamental bands at 469 and 1661 cm^{-1}. In contrast, for the decyl-PQ solution, the combination band at 2127 cm^{-1} is about 5 cm^{-1} less than the sum frequency of the fundamental bands at 469 and 1663 cm^{-1} (see Fig. 4d). This frequency deviation for the combination band can be explained to be due to anharmonicity effect that likely results from the interaction of the quinoid ring with the solvent ethanol [36,37]. The existence of this interaction is indicated from the derivative-shaped spectral features in the region between 900 and 1500 cm^{-1} in Fig. 4d, because those features are formed due to the frequency shift of the signal attributed to ethanol. That is, the anharmonicity effect on the quinoid ring is negligible for the 'other PQs' in PSII membranes. This analysis indicates that the 'other PQs' are likely situated in a hydrophobic environment; therefore, they are probably those PQs in the hydrophobic region of the PSII enzyme or the membrane. Importantly, most of them can be reduced under red light illumination as seen in Fig. 4b. By reverse phase HPLC, 3.2 PQs per reaction center has been determined for BBY preparation [20]. The detection of the 'other PQs' by UVRR spectroscopy in this work thus supports the view that another functional PQ cofactor (not Q_A or Q_B) exists in PSII. For example, Guskov et al. observed another plastoquinone Qc in a cyanobacteria PSII crystal by X-ray diffraction [3,4].

In this work, the molecular vibrations of PSII membranes, in particular the vibrations of the redox-linked carbonyl bonds of PQs therein, are achieved by 257-nm resonance Raman spectroscopy. Using the pump-probe method in combination with a sample jet technique, we can distinguish the signals of different types of PQ cofactors including Q_A, Q_B and the 'other PQs' in the PSII electron transfer chain. This UVRR approach will be useful to the study of quinone molecules in photosynthesis or other biological systems. It is noteworthy that another vibrational spectroscopy, FTIR, has been extensively used to characterize the chemical bonds in PSII. However, for plant PSII, the infrared region around 1660 cm^{-1} overlaps with amide I absorption, making FTIR experiments challenging in this region [21,38]. While the assignment of the Q_A band has been proposed previously [21], this conclusion was based on isotope-editing and FTIR spectroscopy in a congested amide I region. UVRR spectroscopy provides a more selective approach in which the Q_A and Q_B bands are observable without the incorporation of isotopes.

In conclusion, pump-probe 257-nm resonance Raman investigations unambiguously present the carbonyl vibration signals of PQs in PSII

membranes. A strong band at 1661 cm^{-1} is assigned to ring C═C/C═O symmetric stretch mode (ν8a mode) of PQ. The signals of Q_A and Q_B are distinguished, with ν8a mode at 1658.7 and 1660.1 cm^{-1}, respectively. This frequency difference of 1.4 cm^{-1} in ν8a mode between Q_A and Q_B suggests ~86 mV redox potential difference imposed by their protein environment. In addition, we detected the 'other PQs' in the PSII membranes, with ν8a mode at 1661.2 cm^{-1}. A negligible anharmonicity effect on the combination band at 2130 cm^{-1} suggests that the 'other PQs' are situated in a hydrophobic environment. The detection of the 'other PQs' supports the view that another functional PQ cofactor (not Q_A or Q_B) exists in PSII.

Transparency document

The Transparency document associated with this article can be found, in the online version.

Acknowledgements

This work was supported by National Natural Science Foundation of China (31100618), the '100 talent fund' from the Chinese Academy of Sciences for building the 257-nm Raman instrument, and the U.S. National Science Foundation, MCB 1411734 (B.A.B.).

Appendix A. Supplementary data

Supplementary data to this article can be found online at http://dx.doi.org/10.1016/j.bbabio.2015.03.002.

References

[1] B. Nowicka, J. Kruk, Occurrence, biosynthesis and function of isoprenoid quinones, Biochim. Biophys. Acta Bioenerg. 1797 (2010) 1587–1605.
[2] N. Nelson, C.F. Yocum, Structure and function of photosystems I and II, Annu. Rev. Plant Biol. 57 (2006) 521–565.
[3] A. Guskov, J. Kern, A. Gabdulkhakov, M. Broser, A. Zouni, W. Saenger, Cyanobacterial photosystem II at 2.9-angstrom resolution and the role of quinones, lipids, channels and chloride, Nat. Struct. Mol. Biol. 16 (2009) 334–342.
[4] F. Muh, C. Glockner, J. Hellmich, A. Zouni, Light-induced quinone reduction in photosystem II, Biochim. Biophys. Acta Bioenerg. 1817 (2012) 44–65.
[5] T. Cardona, A. Sedoud, N. Cox, A.W. Rutherford, Charge separation in Photosystem II: a comparative and evolutionary overview, Biochim. Biophys. Acta Bioenerg. 1817 (2012) 26–43.
[6] R. de Wijn, H.J. van Gorkom, Kinetics of electron transfer from Q_A to Q_B in photosystem II, Biochemistry 40 (2001) 11912–11922.
[7] Y. Umena, K. Kawakami, J.R. Shen, N. Kamiya, Crystal structure of oxygen-evolving photosystem II at a resolution of 1.9 angstrom, Nature 473 (2011) 55–60.
[8] K. Saito, A.W. Rutherford, H. Ishikita, Mechanism of proton-coupled quinone reduction in Photosystem II, Proc. Natl. Acad. Sci. U. S. A. 110 (2013) 954–959.
[9] G. Balakrishnan, C.L. Weeks, M. Ibrahim, A.V. Soldatova, T.G. Spiro, Protein dynamics from time resolved UV Raman spectroscopy, Curr. Opin. Struct. Biol. 18 (2008) 623–629.
[10] S.A. Oladepo, K. Xiong, Z.M. Hong, S.A. Asher, J. Handen, I.K. Lednev, UV resonance Raman investigations of peptide and protein structure and dynamics, Chem. Rev. 112 (2012) 2604–2628.
[11] X.J. Zhao, H. Imahori, C.G. Zhan, Y. Mizutani, Y. Sakata, T. Kitagawa, Ultraviolet resonance Raman spectra and ab initio vibrational analyses of 1,4-benzoquinone: reassignments of the nu(2) and nu(3) bands, Chem. Phys. Lett. 262 (1996) 643–648.
[12] X.J. Zhao, H. Imahori, C.G. Zhan, Y. Sakata, S. Iwata, T. Kitagawa, Resonance Raman and FTIR spectra of isotope-labeled reduced 1,4-benzoquinone and its protonated forms in solutions, J. Phys. Chem. A 101 (1997) 622–631.
[13] X.J. Zhao, T. Kitagawa, Solvent effects of 1,4-benzoquinone and its anion radicals probed by resonance Raman and absorption spectra and their correlation with redox potentials, J. Raman Spectrosc. 29 (1998) 773–780.
[14] M.L. Josien, N. Fuson, J.M. Lebas, T.M. Gregory, An infrared spectroscopic study of the carbonyl stretching frequency in a group of ortho-quinones and para-quinones, J. Chem. Phys. 21 (1953) 331–340.
[15] N. Fuson, M.L. Josien, E.M. Shelton, An infrared spectroscopic study of the carbonyl stretching frequency in some groups of ketones and quinones, J. Am. Chem. Soc. 76 (1954) 2526–2533.
[16] J. Chen, B.A. Barry, Ultraviolet resonance Raman microprobe spectroscopy of photosystem II, Photochem. Photobiol. 84 (2008) 815–818.
[17] J. Chen, S.L. Bender, J.M. Keough, B.A. Barry, Tryptophan as a probe of photosystem I electron transfer reactions: A UV resonance Raman study, J. Phys. Chem. B 113 (2009) 11367–11370.
[18] S.B. Chang, T.S. Vedvick, A study of plastoquinones in photochemical reactions in chloroplasts of *Euglena gracilis* strain Z, Plant Physiol. 43 (1968) 1661–1665.
[19] A. Melis, J.S. Brown, Stoichiometry of system I and system II reaction centers and of plastoquinone in different photosynthetic membranes, Proc. Natl. Acad. Sci. U. S. A. 77 (1980) 4712–4716.
[20] J.S. Patzlaff, B.A. Barry, Pigment quantitation and analysis by HPLC reverse phase chromatography: a characterization of antenna size in oxygen-evolving photosystem II preparations from cyanobacteria and plants, Biochemistry 35 (1996) 7802–7811.
[21] M.R. Razeghifard, et al., In vivo, in vitro, and calculated vibrational spectra of plastoquinone and the plastosemiquinone anion radical, J. Phys. Chem. B 103 (1999) 9790–9800.
[22] D.A. Berthold, G.T. Babcock, C.F. Yocum, A highly resolved, oxygen-evolving photosystem-II preparation from spinach thylakoid membranes — EPR and electron-transport properties, FEBS Lett. 134 (1981) 231–234.
[23] B.A. Barry, J. Chen, J. Keough, D. Jenson, A. Offenbacher, C. Pagba, Proton-coupled electron transfer and redox-active tyrosines: structure and function of the tyrosyl radicals in ribonucleotide reductase and photosystem II, J. Phys. Chem. Lett. 3 (2012) 543–554.
[24] W.Y. Wang, J. Chen, C. Li, W.M. Tian, Achieving solar overall water splitting with hybrid photosystems of photosystem II and artificial photocatalysts, Nat. Commun. 5 (4647) (2014) http://dx.doi.org/10.1038/ncomms5647.
[25] Y. Yamamoto, M. Doi, N. Tamura, M. Nishimura, Release of polypeptides from highly-active O_2-evolving photosystem-2 preparation by tris treatment, FEBS Lett. 133 (1981) 265–268.
[26] R.K. Mishra, D.F. Ghanotakis, Selective extraction of CP 26 and CP 29 proteins without affecting the binding of the extrinsic proteins (33, 23 and 17 kDa) and the DCMU sensitivity of a photosystem-II core complex, Photosynth. Res. 42 (1994) 37–42.
[27] W. Tian, et al., An irradiation density dependent energy relaxation in plant photosystem II antenna assembly, Biochim. Biophys. Acta Bioenerg. 1847 (2015) 286–293.
[28] B.A. Diner, F. Rappaport, Structure, dynamics, and energetics of the primary photochemistry of photosystem II of oxygenic photosynthesis, Annu. Rev. Plant Biol. 53 (2002) 551–580.
[29] A. Krieger-Liszkay, A.W. Rutherford, Influence of herbicide binding on the redox potential of the quinone acceptor in photosystem II: relevance to photodamage and phytotoxicity, Biochemistry 37 (1998) 17339–17344.
[30] C. Fufezan, C.M. Gross, M. Sjodin, A.W. Rutherford, A. Krieger-Liszkay, D. Kirilovsky, Influence of the redox potential of the primary quinone electron acceptor on photoinhibition in photosystem II, J. Biol. Chem. 282 (2007) 12492–12502.
[31] M.J. Frisch, et al., Gaussian 03, Gaussian, Inc., Pittsburgh, PA, 2003.
[32] H.H. Robinson, A.R. Crofts, Kinetics of the oxidation reduction reactions of the photosystem II quinone acceptor complex, and the pathway for deactivation, FEBS Lett. 153 (1983) 221–226.
[33] A.R. Crofts, C.A. Wraight, The electrochemical domain of photosynthesis, Biochim. Biophys. Acta 726 (1983) 149–185.
[34] J. Minagawa, Y. Narusaka, Y. Inoue, K. Satoh, Electron transfer between Q_A and Q_B in photosystem II is thermodynamically perturbed in phototolerant mutants of *Synechocystis* sp. PCC 6803, Biochemistry 38 (1999) 770–775.
[35] R. Brudler, et al., Asymmetric binding of the 1- and 4-C═O groups of Q_A in *Rhodobacter sphaeroides* R26 reaction centres monitored by Fourier transform infra-red spectroscopy using site-specific isotopically labeled ubiquinone-10, EMBO J. 13 (1994) 5523–5530.
[36] M. Pfeiffer, A. Lau, K. Lenz, T. Elsaesser, Anharmonicity effects in the resonance Raman spectra of heterocyclic aromatic molecules showing photoinduced intramolecular proton transfer, Chem. Phys. Lett. 268 (1997) 258–264.
[37] T. Ebata, K. Nagao, N. Mikami, Mode-dependent anharmonic coupling between OH stretching and intermolecular vibrations of the hydrogen-bonded clusters of phenol, Chem. Phys. 231 (1998) 199–204.
[38] A. Takano, R. Takahashi, H. Suzuki, T. Noguchi, Herbicide effect on the hydrogen-bonding interaction of the primary quinone electron acceptor Q_A in photosystem II as studied by Fourier transform infrared spectroscopy, Photosynth. Res. 98 (2008) 159–167.